Geomorphology xxx (2014) xxx–xxx

Contents lists available at ScienceDirect

Geomorphology

journal homepage: www.elsevier.com/locate/geomorph

Synergy of tectonic geomorphology, applied geophysics and remote sensing techniques reveals new data for active extensional tectonism in NW Peloponnese (Greece)

Ioannis Fountoulis [b,1], Emmanuel Vassilakis [a,*], Spyridon Mavroulis [b], John Alexopoulos [c], Spyridon Dilalos [c], Athanasia Erkeki [d]

[a] National and Kapodistrian University of Athens, Faculty of Geology and Geoenvironment, Department of Geography & Climatology, Panepistimiopolis Zografou 15784, Greece
[b] National and Kapodistrian University of Athens, Faculty of Geology and Geoenvironment, Department of Dynamic Tectonic Applied Geology, Panepistimiopolis Zografou 15784, Greece
[c] National and Kapodistrian University of Athens, Faculty of Geology and Geoenvironment, Department of Geophysics-Geothermy, Panepistimiopolis Zografou 15784, Greece
[d] National and Kapodistrian University of Athens, Faculty of Geology and Geoenvironment, Laboratory of Natural Hazards' Prevention & Management, Panepistimiopolis Zografou 15784, Greece

ARTICLE INFO

Article history:
Received 3 April 2012
Received in revised form 17 November 2014
Accepted 25 November 2014
Available online xxxx

Keywords:
Morphotectonic indices
Fault slip rate
Photogrammetry
Digital shoreline analysis
Vertical Electrical Sounding

ABSTRACT

In tectonically active areas, such as in the northwest Peloponnese of western Greece, geomorphic processes are strongly influenced by active faulting; in many cases such faults cannot be easily identified. In this paper we apply multidisciplinary analysis (morphotectonic indices, neotectonic mapping, geophysical surveys and remote sensing techniques) to map the recently-recognized east–west trending Pineios River normal fault zone with a high degree of accuracy, and to better understand its contribution to the evolution of the ancient region of Elis during Holocene time. Fault activity seems to be related to frequent changes in river flow patterns and to displacements of the nearby shoreline. We argue that fault activity is the main reason for migration of Pineios river mouth as documented for several time periods during historical time. Quantitative constraints on deformation caused by the faulting were applied through the application of the morphotectonic indices proposed in this paper, including drainage network asymmetry and sinuosity, and mountain front sinuosity, all of which indicate that this is a highly active structure. Slip rates calculated to be as high as 0.48 mm/yr for the last 209 ka (based on previously published dating) were verified by applied geophysical methods. The fault surface discontinuity was identified at depth using vertical electrical resistivity measurements and depositional layers of different resistivity were found to be clearly offset. Displacement increases toward the west, reaching an observed maximum of 110 m. The most spectacular landform alteration due to surface deformation is the north–south migration of the river estuary into completely different open sea areas during the late Quaternary, mainly during the Holocene. The sediment transport path has been altered several times due to these changes in river geometry with and the most recent seeming to have occurred almost 2000 years ago. The river estuary migrated to its contemporary position along the southern coast, settled on the hanging wall, inducing retrograding of the northern coast, and settled on the foot wall, with rates reaching the order of 0.52 m/yr, as concluded from historical and recently-acquired remote sensing data.

1. Introduction

The northwest Peloponnese is located along the external part of the Hellenic orogenic arc, a few tens of kilometers internal (east) of the Hellenic trench. It has been repeatedly subjected to large seismic events and earthquake related geo-environmental phenomena, with the latest such event occurring on June 8th 2008 (Mw = 6.4) (Lekkas et al., 2008; Konstantinou et al., 2009; Feng et al., 2010; Koukouvelas et al., 2010; Margaris et al., 2010; Mavroulis et al., 2010, 2013; Papadopoulos et al., 2010). Seismic activity has been recorded continuously in this region throughout historical times (Papazachos and Papazachou, 1997). Thus it is important to understand the slip behavior of faults that have caused or may cause earthquakes in the near future. The Pineios fault zone is a tectonic structure that has only been recently mapped, and it has never been identified as the locus of any historical earthquake (Mavroulis, 2009). It is located in the northwest Peloponnese and has drastically affected the Lower Pineios River plain, along which the ancient Elis developed during Hellenistic and Roman times (Kraft et al., 2005).

Today, the ruins of ancient Elis lie downstream from a man-made dam on the modern Pineios River. Abandonment of this section of the river was probably caused by several geodynamic processes, perhaps related to active tectonism over a wider region (Guidoboni et al., 1994). In this paper we argue that fault activity caused the river estuary to relocate and consequently secondary landform processes affected the broader region surrounding the Lower Pineios River during Upper Quaternary time (Fountoulis et al., 2011, 2013). The combination of methodologies described in this paper includes tectonic–geomorphic

* Corresponding author.
[1] Deceased.

http://dx.doi.org/10.1016/j.geomorph.2014.11.016
0169-555X/

analysis, applied geophysical measurements and remote sensing techniques and are designed to (a) assess the tectonic activity of Pineios fault zone, (b) provide quantitative information on the fault activity, (c) clarify the stratigraphic sequences beneath the study area, (d) accurately map the fault zone at depth and estimate its displacement, and (e) quantify the influence of the active faulting on the coastal environment.

2. Geological setting

The westernmost part of Peloponnese is an area with generally low relief (Fig. 1) and is mostly covered by recently deposited sediments (Kamberis et al., 1993). Post-alpine sedimentary sequences that are observed throughout the Pyrgos–Olympia basin are Pliocene and Quaternary in age and lie unconformably on the deformed alpine basement. Their geographical distribution and variety of facies (marine, lagoonal, lacustrine and terrestrial) clearly reflect young vertical fault block movements and ongoing active tectonism (Lekkas et al., 1992). Using published geological mapping (Kamberis et al., 1993), paleontological observations (Athanassiou, 2000), and $^{230}Th/^{238}U$ dating of corals found in the marine terraces of the northwest Peloponnese (Stamatopulos et al., 1988), a typical stratigraphic section for the post-alpine succession can be constructed and demonstrates post-Pliocene paleo-environment changes. Specifically, the sediment sequence consists of: (a) lacustrine and lagoonal marls of Upper Pliocene–Pleistocene age, (b) shallow marine sands, sandstones and conglomerates of Pleistocene age, (c) marine calcareous sandstones of Pleistocene age, and (d) Holocene alluvial deposits (sands, gravels) of the Lower Pineios River valley that unconformably overlie the formations (a–c). Plio-Pleistocene molluscan assemblages and sedimentary facies indicate a

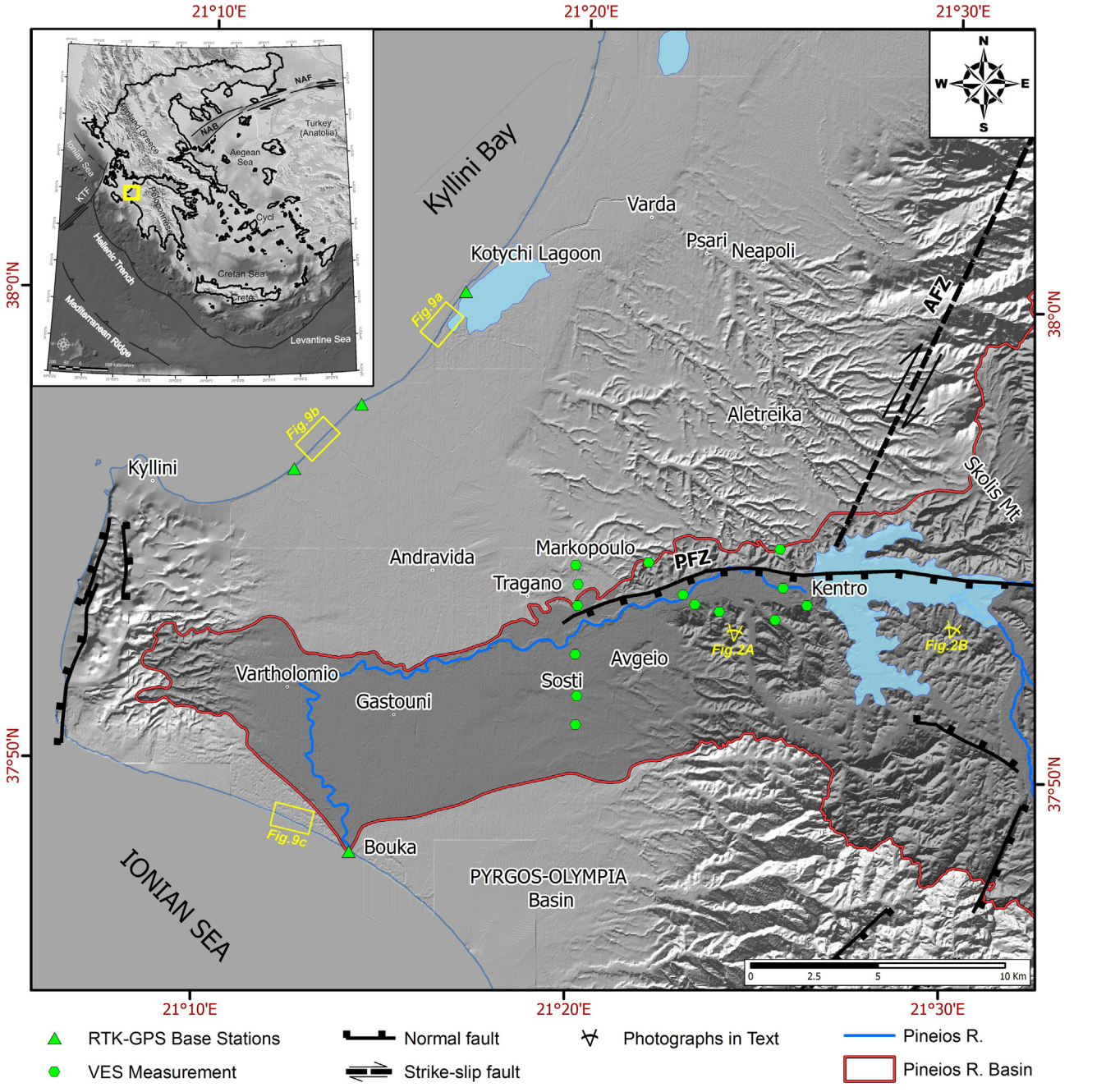

Fig. 1. Index map of the study area in the northwest Peloponnese. The trace of the active fault zone described in this paper is shown immediately north of the Pineios River. This active fault zone is responsible for a number of landform processes as described in the text.

Please cite this article as: Fountoulis, I., et al., Synergy of tectonic geomorphology, applied geophysics and remote sensing techniques reveals new data for active extensional tecton..., Geomorphology (2014), http://dx.doi.org/10.1016/j.geomorph.2014.11.016

continuous alternation of shallow marine, brackish and lacustrine environments (Paraskevaidis and Symeonidis, 1965). The broader region of the Pineios valley has produced fossil Mammals, including Hippopotamus (Thenius, 1955; Symeonidis and Therodorou, 1986) and Elephas (Kamberis, 1987; Athanassiou, 2000) specimens have been discovered, indicating a pre-existing fluvial-lacustrine environment. Using deep borehole data, Kamberis et al. (1993) demonstrated that the maximum thickness of the post-alpine sequence exceeds 3000 m and unconformably covers the basement rocks.

The alpine basement comprises three alpine tectonic units; thin bedded pelagic sediments of the Pindos unit are found overthrust onto neritic carbonates and flysch of the Gavrovo–Tripolis unit, which are in turn overthrust onto evaporites, limestones and flysch of the Ionian unit, which is the most external unit of the external Hellenides (Papanikolaou, 1984, 1997).

2.1. Regional active tectonics

The Ionian Islands and the Gulf of Corinth are included in the most seismic and tectonically active regions in Greece (Hatzfeld et al., 1990). The Peloponnese lies at the junction of those rapidly evolving areas (Vassilakis et al., 2011). Intense tectonic activity in this region has been continuous from Miocene until Holocene time (Hollenstein et al., 2006 and references therein) and is related to its position in the external part of the active Hellenic forearc and its proximity to the present day NNW–SSE trending Hellenic trench which is an active subduction boundary separating the African and the European plates. Additionally, ongoing diapirism of Triassic evaporites of the Ionian unit amplifies the deformation of this region in a non-systematic way (Underhill, 1988).

Several active faults were studied; some of these were active previously (e.g., in Pliocene or Pleistocene time) whereas some were still active in Holocene time (Mariolakos et al., 1991; Lekkas et al., 1992). The recorded seismicity level, which is possibly one of the highest in the Mediterranean regions (Hatzfeld et al., 1990), supports the neotectonic observations and indicates that the broader area is undergoing intense tectonic deformation. According to historical and instrumental records, numerous destructive earthquakes have taken place in the area since 399 BC, most, if not all, of which were shallow (<20 km) and have been assigned high intensities (Papazachos and Papazachou, 1997).

The neotectonic structure of northwestern Peloponnese is characterized by large, independently-moving blocks that form grabens and horsts bounded by fault zones, which may be visible or concealed. These extensional structures trend mainly east–west or north-northwest and create a complex matrix of neotectonic blocks with particular evolution characteristics and relative displacements (Mariolakos et al., 1985). Sedimentation processes in the area have been highly influenced by the dominant neotectonic regime and faulting is reflected in the sedimentary structures (Papanikolaou et al., 2007).

The large-scale neotectonic structures of the study area are the faults that define the Pyrgos–Olympia post-alpine basin, which covers an area of 1500 km^2. The marginal fault zones are clearly discernible and form impressive morphological discontinuities (Lekkas et al., 1992, 2000; Fountoulis et al., 2007). The basin itself is filled with post-alpine deposits of Late Miocene to Holocene age, reaching a thickness of approximately 3 km (Kamberis, 1987).

The trace of the Pineios normal fault zone is observed south-southwest of Skolis Mt and was not identified until recently (Mavroulis, 2009). It is generally east–west trending and dips southwards. Its surface expression coincides with a slightly degraded but clearly observable morphological discontinuity that extends eastwards from the northernmost banks of the Pineios artificial lake and westwards to Tragano village (Fig. 2). The footwall consists of post-alpine formations of Upper Pliocene to Pleistocene age unconformably overlying the paleo-relief developed on top of the alpine basement. The hanging wall consists of the same post-alpine formations partially covered by alluvial deposits of the Pineios River.

It is noteworthy that the post-alpine formations of the footwall form a broad Tyrrhenian marine terrace consisting of sands, sandstones and conglomerates which outcrop north and south of the fault zone over an area of hundreds of square kilometers (Stamatopulos et al., 1988). The terraced surface forms a monocline dipping northwestwards as indicated by strike and dip measurements obtained during general geological fieldwork (Mavroulis, 2009; Mavroulis et al., 2010). In particular, Pleistocene marine formations of the footwall dip northwestwards between 4° and 14° while the Upper Pliocene to Pleistocene marine and lagoonal formations that crop out at the hanging wall dip northwestwards between 7° and 30°. These fossiliferous marine deposits are commonly found under a thin cover of reddish sandy and conglomeratic alluvial deposits.

Fieldwork in the region surrounding the Lower Pineios River reveals significant geomorphic evidence of recent tectonic activity (Mavroulis, 2009; Mavroulis et al., 2010; Fountoulis et al., 2011, 2013; this study). The most diagnostic tectonic landforms associated with Pineios fault zone are successive sets of slightly degraded but well-defined and well-preserved triangular facets along the morphological discontinuity formed by the fault zone (Fig. 2). These tectonic landforms indicate active faulting with a normal component of displacement (Wallace, 1977; Menges, 1990). They reflect rapid, recent and cumulative uplift, as only such movements can maintain such features in this landscape where the lithologies present are dominantly porous marine calcareous sandstones, marine sands, sandstones, conglomerates, lacustrine and lagoonal clays. The formation and preservation of such landforms are consistent with rapid recent uplift of the footwall over a period lasting from 10^3 to 10^6 years (Cotton, 1950; Bull, 1978). Therefore, rapid extensional tectonic activity appears to be present along this mountain front and the process of forming the triangular facets should be quite recent.

Note that there has been no indication of rupture along the Pineios fault system after the damaging earthquake of June 2008 (Konstantinou et al., 2009; Feng et al., 2010; Koukouvelas et al., 2010). However, a significant number of rock falls were observed along the triangular facets as shown in Fig. 2a, as well as post-seismic liquefaction around the artificial lake (Mavroulis et al., 2013).

3. Morphotectonic analysis of the Pineios fault zone using morphometric indices

Bull and McFadden (1977) introduced the quantitative analysis of the topography as a tool for evaluating active faulting. Simple ratios between particular landform observables can serve as a valuable tool for tectonic geomorphology studies along faulted mountain fronts. These metrics include mountain–piedmont junction sinuosity, percentage of triangular faceting along mountain fronts, longitudinal river profile analyses and variations of valley-floor slopes.

3.1. Mountain front sinuosity (S_{mf})

Mountain front sinuosity (S_{mf}) is an index that describes the degree of irregularity or sinuosity along the base of a topographic escarpment. The parameter is useful because of the tendency of active structures to maintain straight or curvilinear profiles in map view, in contrast to the more irregular profiles produced by erosional processes along the base of non-fault related topographic escarpments. Mountain front sinuosity (S_{mf}) is defined as the ratio of the observed length along the margin of the topographic mountain–piedmont junction (L_{mf}) to the overall length of the mountain front (L_s) and is defined as: $S_{mf} = L_{mf} / L_s$ (Bull and McFadden, 1977; Bull, 1978). This index has been applied in a variety of active geologic environments throughout the world; the most tectonically active mountain fronts are characterized by values of S_{mf} ranging from 1.0 to 1.4 (Bull and McFadden, 1977; Rockwell et al., 1984; Wells et al., 1988; Theocharis and Fountoulis, 2002; Silva et al.,

Please cite this article as: Fountoulis, I., et al., Synergy of tectonic geomorphology, applied geophysics and remote sensing techniques reveals new data for active extensional tecton..., Geomorphology (2014), http://dx.doi.org/10.1016/j.geomorph.2014.11.016

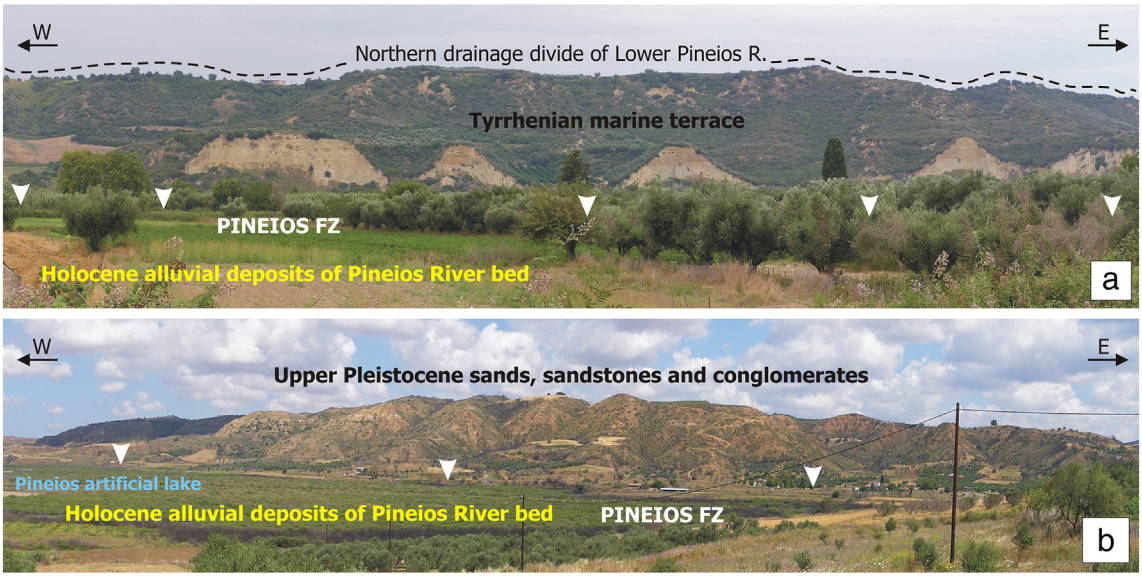

Fig. 2. (a) Partial view of the area downstream of the artificial dam, looking toward the Pineios fault zone (Pineios FZ). In this segment of the fault zone the footwall consists of Tyrrhenian marine terrace sediments, while Holocene alluvial deposits of the Pineios riverbed cover the hanging wall. (b) Partial view of the area upstream of the artificial dam, looking toward the Pineios fault zone (Pineios FZ). Well-preserved triangular facets are developed on the Upper Pleistocene deposits. In both photographs the white arrowheads point to the fault trace.

2003). Wells et al. (1988) argue that values of S_{mf} above 1.4 cannot be unambiguously interpreted in terms of active faulting. Values of S_{mf} greater than 3 are normally associated with mountain fronts with decreased amounts of tectonic uplift relative to basal erosion, such as where the primary range-front fault is more than 1 km from the erosional front (Bull and McFadden, 1977).

Values of S_{mf} depend, among other factors, on topographic scale; small-scale topographic maps produce only a rough estimate of mountain front sinuosity. Therefore we measured mountain front sinuosity and other morphometric variables on large-scale topographic maps (1:5000, with 4 m contour intervals) published by the Hellenic Military Geographical Service (HMGS).

Mountain front sinuosity was measured in three segments of the morphological discontinuity located immediately north of Pineios valley and downstream of the artificial lake and their distinction was based on the hill-front general slope direction change (Fig. 2). Values of L_{mf}, L_s and S_{mf} are given in Table 1 and S_{mf} values depicted in Fig. 3a. Calculated S_{mf} values range from 1.23 to 1.32, indicating that the hill front formed by the Pineios fault zone is tectonically active (Bull and McFadden, 1977; Rockwell et al., 1984; Wells et al., 1988; Silva et al., 2003).

3.2. Percentage of faceting along mountain front (F%)

The facet index (F%) is the percentage of a given mountain front with well-shaped triangular facets. It is defined as the ratio of the cumulative length of facets (L_f) to the length of the mountain front (L_s) (Bull, 1978; Wells et al., 1988). A high percentage of faceting along the mountain front indicates tectonic activity (Ramírez-Herrera, 1998). Potential difficulties with the application of this morphometric index are the systematic definition of an individual facet and the discrimination between faceted and non-faceted sections of a mountain front (DePolo and Anderson, 2000). To mitigate these difficulties, topographic maps of 1:5000 published by the HMGS were also used.

The percentage of faceting along the mountain front (F%) was measured in each of the three segments developed north of Pineios valley (see Section 3.1). Values of L_f, L_s and F% for each segment are given in Table 1 and F% is also depicted in Fig. 3b. F% values range from 56% to 80%, indicating tectonic activity along the hill front of Pineios fault zone.

Table 1
Mountain front sinuosity (S_{mf}) and percentage of faceting along the hill front (F%) for Pineios fault zone. Segments A, B, and C are depicted in Fig. 3.

Pineios FZ segments	L_{mf} (in m)	L_s (in m)	S_{mf}	ΣL_f (in m)	L_s (in m)	F	F%
A	2926.97	2215.92	**1.32**	1230.89	2215.92	0.56	**56**
B	7738.86	6202.62	**1.25**	4598.71	6202.62	0.74	**74**
C	3595.13	2921.51	**1.23**	2340.74	2921.51	0.80	**80**

The bold numbers refer to the calculated values. The normal numbers refer to the measurements.

3.3. The alluvial river response to Pineios fault zone

3.3.1. Asymmetry of the Lower Pineios River network

The river valley adjacent to the main Pineios fault zone trends in an E–W direction and crosses Pliocene and Pleistocene formations. Activity along the Pineios fault zone appears to have caused differential vertical motion of several fault blocks accompanied by block-tilting in a cross-valley direction. Tilting of fault blocks and northward migration of the Lower Pineios River valley have in turn caused asymmetry of the drainage network developed on top of the hanging wall. Thus, the river has shifted gradually northwards and flows adjacent and parallel to the northern drainage divide (Fig. 2). This asymmetrical development is clearly reflected by the number, size and order of the tributaries and sub-basins on either side of the river. North of the Lower Pineios River (7th order), 1st and 2nd order drainage basins prevail, while higher order drainage basins are less common and significantly smaller (Fig. 4). In contrast, 3rd order drainage basins are much larger and cover an extensive area to the left of the main branch of the river, downstream from the artificial lake. This asymmetric development of sub-basins reflects block rotation during tectonism (Cox, 1994; Garrote et al., 2006) and is in full agreement with the observations made during fieldwork (Mavroulis, 2009).

3.3.2. Longitudinal profile of Lower (alluvial) Pineios River and valley floor slope changes

The longitudinal profile of the Lower Pineios River, from the Kentro area (upstream) to the Bouka area (downstream) at the contemporary river mouth, was obtained from a high resolution (2-meter) Digital Elevation Model (DEM), constructed after photogrammetric processing of available aerial photographs. The river profile was segmented into three parts, (a) upstream, (b) intermediate and the (c) downstream segments (Fig. 4). The upstream segment of the profile (from point K

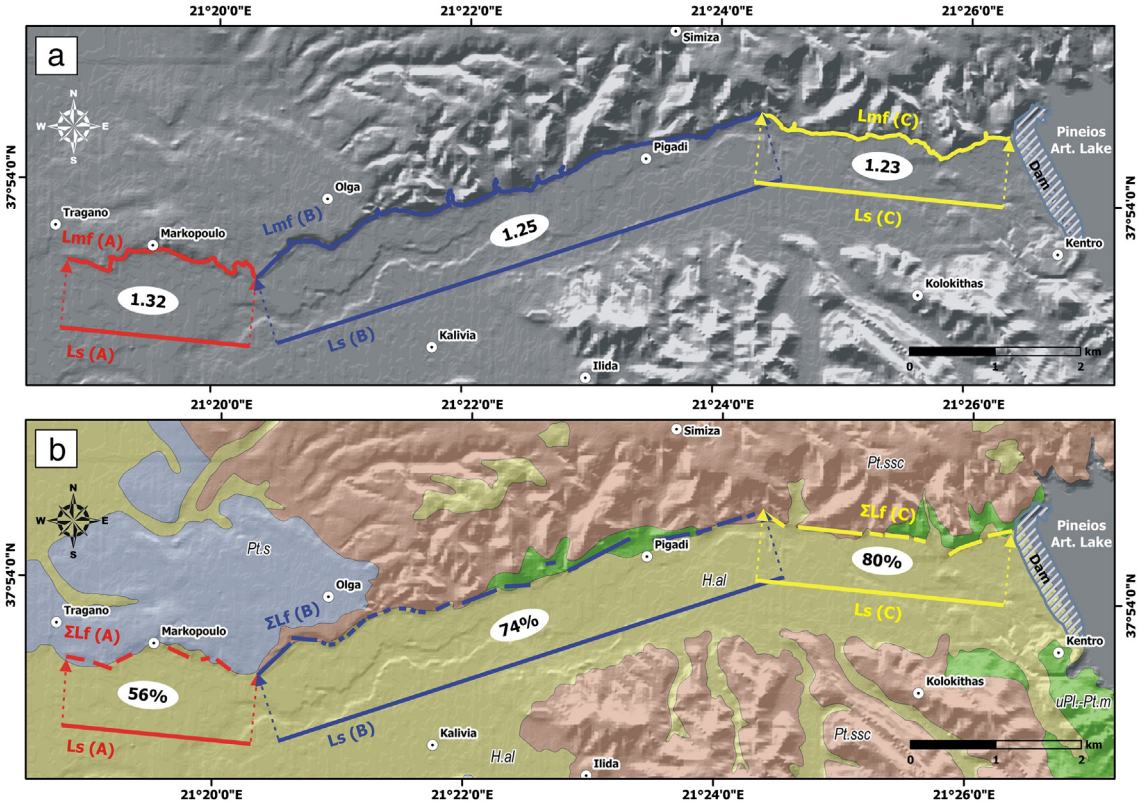

Fig. 3. (a) Mountain front sinuosity (S_{mf}) values for the three segments of the morphological break located north of the Pineios valley are shown in the white ellipses and range from 1.23 to 1.32. These values indicate that the Pineios fault zone is an active tectonic structure (Bull and McFadden, 1977; Rockwell et al., 1984; Wells et al., 1988; Silva et al., 2003). (b) Percentage of faceting along the mountain front: these values of 56–80% are clear indicators of active faulting. (H.al: Holocene deposits, Pt.s: Pleistocene calcareous sandstones, Pt.ssc: Pleistocene sands, sandstones and conglomerates, uPl.–Pt.m: Upper Pliocene–Pleistocene marls).

to point M) corresponds to the east–west trending part of the Lower Pineios River, extending westwards from the Kentro area (upstream) to Markopoulo (downstream). The valley-floor slope of the upstream segment was measured at 0.36%. The intermediate segment of the profile (from point M to point V) corresponds to the east–west trending part of the Lower Pineios River, extending eastwards from Markopoulo (upstream) to the Vartholomio area (downstream). The valley-floor slope of the intermediate segment was measured at 0.10%. The downstream segment (from point V to point B) corresponds to the north–south trending and gently sloping lower course of the Lower Pineios River, extending southwards from the Vartholomio area (upstream) to the Bouka area (Pineios River mouth). The valley-floor slope of the downstream segment was measured at 0.056%.

The valley-floor slope of the upstream river segment (0.36%) is almost 4 times greater than that of the intermediate segment (0.10%) and almost 6 times greater than that of the downstream segment (0.056%). Furthermore, the valley floor slope of the intermediate segment is twice that of the downstream segment. Point M, where the first significant change of the valley floor slope is situated, is very close to the westernmost edge of the morphological discontinuity along the mountain front (Fig. 4). The V point, where the second significant change of the valley floor slope is situated, is located very close to the Vartholomio area, where the southward bend of the Lower Pineios River course occurs. This bend in the river course seems to have tectonic origin because it is located at the possible westwards prolongation of the Pineios fault zone. Alternatively, it may be due to diapiric phenomena because the river valley seems to be diverted by the uplifted Kyllini peninsula, which is formed above an evaporitic dome (Kamberis, 1987) and bounds the Gastouni graben. Thus it seems likely that the subsurface tectonic deformation of this area has affected the longitudinal river profile and significant breaks in the longitudinal profiles are areas that appear to be related to active faulting.

3.3.3. Sinuosity index (SI)

Under certain conditions, alluvial rivers evolve as single meandering channels (Brice, 1964; Rust, 1978). This behavior is generally influenced by tectonic movements and is reflected in river channel parameters (Zámolyi et al., 2010). It is generally accepted that if the footwall of an active normal fault lies in the downstream flow direction, it results in increased meandering (Ouchi, 1985; Keller and Pinter, 1996; Holbrook and Schumm, 1999; Bridge, 2003). Provided that the fluvial system is already in the meandering stage, this phenomenon is largely independent of river size. Thus not only large rivers, but smaller creeks and reaches, are suitable for analysis provided that they are essentially free of human influence. Increasing use of Geographic Information Systems (GIS) and the increasing quality of elevation data make calculations of river sinuosity sensitive to neotectonic activity in low-relief areas because even small changes in the topography affect the sinuosity of low gradient rivers (Holbrook and Schumm, 1999).

The sinuosity index (SI) of modern river channels was defined by Leopold and Wolman (1957) as the ratio of the thalweg length to the valley length. Subsequently Brice (1964) suggested a slightly modified sinuosity index (the ratio of the channel length to the length of the meander-belt axis), which has the advantage of allowing for both straight reaches and sinuous meander belts. In both studies, an arbitrary value of 1.5 was used to distinguish between low- and high-sinuosity channels. Although other classification schemes have been described (Schumm, 1963), this value is generally accepted.

The SI values for the Lower Pineios River were calculated using high resolution DEM data derived from photogrammetric processing of aerial photographs. The calculations were made in close proximity to the

Please cite this article as: Fountoulis, I., et al., Synergy of tectonic geomorphology, applied geophysics and remote sensing techniques reveals new data for active extensional tecton..., Geomorphology (2014), http://dx.doi.org/10.1016/j.geomorph.2014.11.016

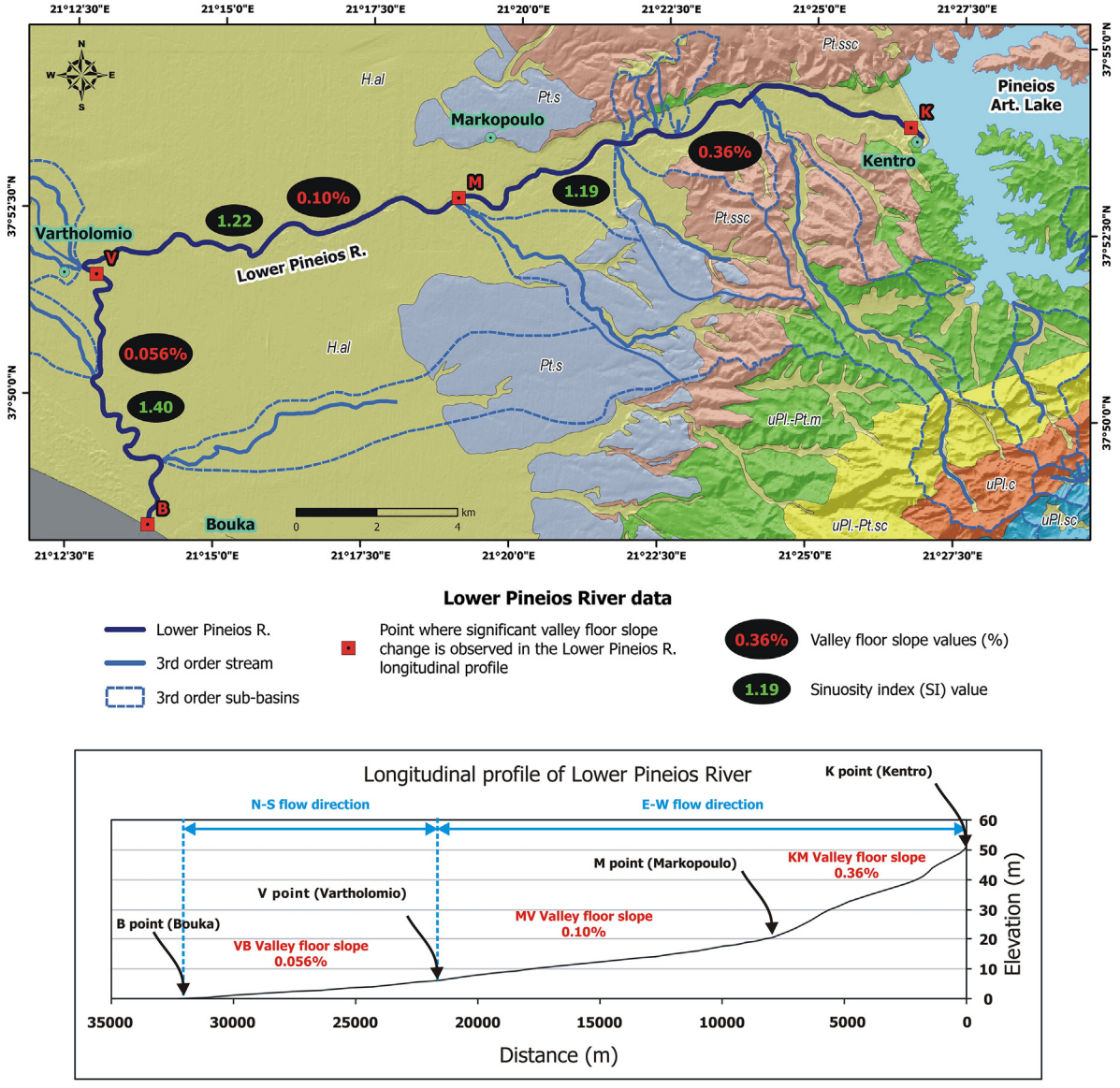

Fig. 4. Significant changes are observed in the valley floor slope (%) and sinuosity index (SI) measured along a longitudinal river profile of the Lower Pineios River. The 3rd order drainage basins prevail south of the 7th order Lower Pineios River, while they are less common north of the main branch of the Pineios River. (H.al: Holocene deposits, Pt.s: Pleistocene calcareous sandstones, Pt.ssc: Pleistocene sands, sandstones and conglomerates, uPl.–Pt.m: Upper Pliocene–Pleistocene marls, uPl.–Pt.sc: Upper Pliocene–Pleistocene sands and clays, uPl.c: Upper Pliocene conglomerates, uPl.sc: Upper Pliocene sands and conglomerates).

northern and western tectonic boundaries of the Gastouni graben, which correspond to the active Pineios fault zone and to Kyllini hill. This is precisely the area where the Lower Pineios River flows and contains the three river segments characterized by different valley floor slope values (see Section 3.3.2).

The sinuosity index and values of the channel length (S — curvilinear distance measurement along the center of the channel) and valley length (L — horizontal distance measured in the thalweg of two cross sections in a linear depression between two adjacent uplands) are given in Table 2.

Table 2
Sinuosity index (SI) and valley floor slope values calculated for Lower Pineios River. Parts KM, MV, and VB are depicted in Fig. 4.

Lower Pineios River part	S (in m)	L (in m)	SI	Valley floor slope (%)
KM	13,154	11,354	**1.19**	**0.36**
MV	11,206	9175	**1.22**	**0.10**
VB	8930	6340	**1.40**	**0.056**

From the upstream (K–M) to the downstream (V–B), the Lower Pineios River valley-floor slope decreases from 0.36% to 0.056%, while sinuosity index values increase from 1.19 to 1.40. It is plausible that sinuosity variations along the Lower Pineios River are related to, or strongly coupled to, differential tectonic deformation and differential uplift/subsidence patterns. This is in full agreement with the thickness and the isobaths of Neogene and Quaternary formations as described by Kamberis (1987). Thus it appears that the Lower Pineios River has responded to active faulting by local changes in its sinuosity (Fig. 4).

4. Uplift rates of fault blocks and Pineios fault slip rate

The study area consists mainly of a succession of Pliocene to Holocene sediments. $^{230}Th/^{238}U$ dating of corals from the upper layers of the sequence indicates a Tyrrhenian age for samples spanning three complete sections from the footwall of the Pineios fault zone (Stamatopulos et al., 1988). The deposition ages were determined to be 103 ka for the Psari section (at an elevation of 40–45 m above sea-level (a.s.l.)), 118 ka for the Neapolis section (at an elevation of 60–

65 m (a.s.l.)) and 209 ka for the Aletreika section (at an elevation of 140–145 m (a.s.l.)). The sampling sites that are located north of Pineios fault zone should be located on a single fault block because there is no sign of tectonic disruption between them (Fig. 1).

The ages of these dated samples correspond to oxygen isotope stages 5.3, 5.5 and 7.3 (Imbrie et al., 1984; Shackleton et al., 1984; Waelbroeck et al., 2002 and references therein). These stages represent high sea-level stands for the Mediterranean Sea (Caputo, 2007) and especially for the western coast of Peloponnese (Athanassas and Fountoulis, 2013). In particular, at 103 ka sea-level was ~13 m below present sea-level, at 118 ka it was ~1 m below present sea-level and at 209 ka it was ~7 m below present sea-level (Waelbroeck et al., 2002).

From the age of each sample and the sea-level change that has occurred since deposition, uplift rates for the footwall of the Pineios fault zone were calculated as ~0.26 mm/yr for the Psari area, ~0.50 mm/yr for the Neapoli area and ~0.64 mm/yr for the Aletreika area (Fountoulis et al., 2011, 2013). The maximum uplift rate of 0.64 mm/yr occurs in close proximity to the fault zone. The areas with lower uplift rates are located much further to the north (Fig. 1). Because all sample locations are inferred to be within the same fault block, this implies back tilting of the fault block toward north, in full agreement with the rotational block-faulting inferred from structural studies based on field-work in the surrounding area.

The rate of uplift for the hanging wall was estimated at ~0.16 mm/yr based on a deposition age of 209 ka and a present elevation of 40 m (a.s.l.), which is the lowest elevation that outcrop of Tyrrhenian sediments is found, considering the sea-level change after the deposition. This is much slower even than the slowest measured rate of footwall uplift rate (0.26 mm/yr). The difference between the uplift rate at Aletreika (in the footwall) and the Pineios River plain (in the hanging wall) is ~0.48 mm/yr; this figure corresponds to the slip rate on the Pineios fault zone over the last 209 ka, indicating an overall throw of the fault of ~100 m.

5. Geoelectrical investigation

A geophysical survey was carried out at the area of Pineios river valley, downstream of the artificial dam, to investigate the boundaries between (i) Holocene fluvial deposits and underlying strata, (ii) Upper Pleistocene sandstones and older conglomeratic layers and (iii) Pleistocene conglomerates and Pliocene lagoonal marls, which is the layer succession described for the broader area by Kamberis et al. (1993). This included Vertical Electrical Sounding (VES), which has been applied successfully to investigation of geological-tectonic structure in other areas (Alexopoulos et al., 2001; Asfahani and Radwan, 2007; Papadopoulos et al., 2007; Alexopoulos and Dilalos, 2010), and has sometimes been combined with morphotectonic surveying (Asfahani et al., 2010). A grid of Vertical Electrical Soundings (VESs) was distributed over an area spanning both blocks because a fault zone might have been present underneath the Holocene deposits near the northern side of the Pineios riverbed. The geoelectrical data acquisition included two "in-situ" resistivity measurements on surface outcrops and thirteen Vertical Electrical Soundings (see Fig. 1 for VES site locations or the Supplementary KMZ file).

5.1. Geophysical–geological calibration

In order to calibrate and better evaluate the geoelectrical results, "in-situ" resistivity measurements were carried out above known outcrops of the existing geological formations. Sites were selected above marls (A3) and sands–sandstones (M1), applying the Schlumberger array, with a maximum AB length equal to 430 m (Fig. 5). This technique contributed to a restrict definition of the corresponding resistivity value limits of the most important geological formations in the area, especially the Plio-Pleistocene lagoonal marls (Table 3). Analysis of survey measurements yielded resistivity values of approximately 20–25 Ω.m for the marls, 57–60 Ω.m for the Pleistocene sand, sandstones and conglomerates and 9–17 Ω.m for the alluvium layers.

5.2. Acquisition and processing of geophysical data

The Schlumberger array configuration was used to make thirteen resistivity soundings. The maximum current electrode spacing (AB) was 1632 m for most of the sites, which were distributed along three sections with different orientations (mainly N–S) in an attempt to cross over normally the morphological escarpment north of Pineios river valley. Several difficulties were encountered during the current electrode spreading operation, mainly due to occasionally steep relief, the residual riverbed, local water pits and various constructions like streets, fences, etc. The equipment used for the field measurements included an ABEM Terrameter SAS300C and a Booster 2000.

The geophysical data were processed by applying the automatic method of Zohdy (1989), composing a "multilayer" model. The Interpex commercial software package IX1D (v.3.5) was used to produce the "layered" model. In almost all soundings, a formation with resistivity values between 20 and 28 Ω.m was detected as the geoelectrical basement (deepest formation) and, based on the "in-situ" measurements, assigned to the Upper Pliocene–Pleistocene marls.

In order to determine the lateral inhomogeneity of the geological formations, a distributed apparent resistivity section was created. These types of sections, based on the processing of original field data without the intervention of processing algorithms, are commonly used to generate quantitative results that illustrate the complexity of the stratigraphic structure. After combining an initial representation we set the criteria for the reliability of the applied 1-D geoelectrical soundings. The qualitative representation and adumbration of the general subsurface structure, three sections of distributed (true) resistivity were created from the results of the multi-layered models (Zohdy, 1989), which includes topographic relief in the processing (Fig. 6). Layered sections were created from the 1-D processing geoelectrical

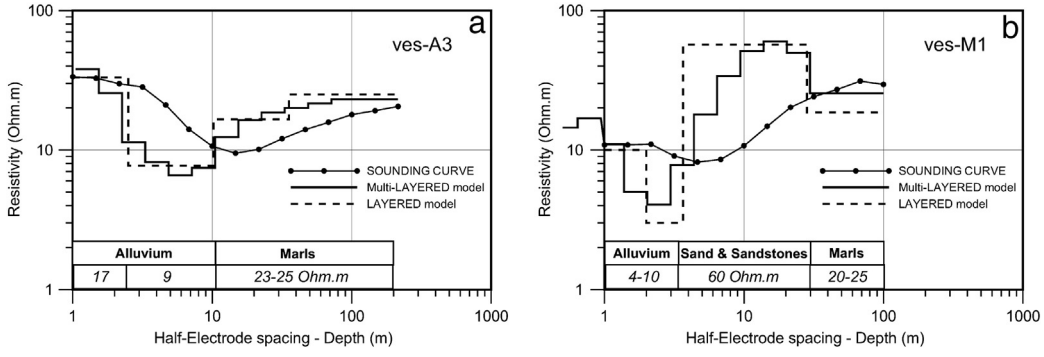

Fig. 5. Indicative interpretation results for VES A3 (a) and M1 (b) where several layers of varying electrical resistivity were detected.

Table 3
Resistivity values after the "in situ" geoelectrical measurements.

Geological formation	Resistivity (Ω.m)
Upper Pliocene–Pleistocene marls (uPl.–Pt.m)	20–25
Pleistocene sands, sandstones and conglomerates (Pt.ssc)	57–60

models that were calculated. Subsequently, the calculated thicknesses of the geoelectrical layers were placed at the proper absolute elevations and the subsurface structure, corresponding to the geoelectrical layers, was obtained for each section. The most significant observation was a clearly defined lateral discontinuity at a distance of about 2900 m in Section C, while in Section A another lateral geoelectrical discontinuity appears to be present at about 750 m (Fig. 6). All other geoelectrical structures seem to consist of homogeneous layering with the apparent resistivity values decreasing with depth.

5.3. Geophysical–geological conclusions

The geophysical data acquired from the study area were combined with the surface geological observations and with the "SOSTI" borehole stratigraphic column published by Kamberis et al. (1993). This is represented in three geoelectrical–geological sections (Fig. 7) crossing almost perpendicularly the Pineios River valley at different orientations (mainly N–S).

Along these sections the boundaries between four different geological formations can be observed, one of which is the geoelectrical basement of the Upper Pliocene–Pleistocene marls (resistivity values of 20–28 Ω.m). This dips 10° northwest, in agreement with measured surface bedding (Mavroulis, 2009). The Pleistocene sand, sandstone and conglomerate formation (>40 Ω.m) can be identified above the marls with a constant thickness of about 100 m in every section. The Pleistocene calcareous sandstones appear at the highest elevations in the northernmost parts of the three sections and south of Pineios riverbed in Section C. The resistivity contrast between the latter two formations was low and there were difficulties in distinguishing them, but through detailed and accurate field observations along the morphological discontinuity north of the Pineios River depression these ambiguities were resolved.

Results from the geophysical sections showed the lateral discontinuity to be a normal fault zone that clearly interrupts the subsurface layers (Figs. 6, 7). The fault displacement, based on offset of the top of the Plio-Pleistocene marls, grows from east (~60 m on Section A) to west (~110 m on Section C) in full agreement with the surface geological data. The uppermost layer of Holocene deposits shows an increasing thickness from east (~10 m) to west (~60 m), also in agreement with the increasing throw along the fault zone to the west.

6. Remote sensing data and shoreline displacement analysis

Toward the west, the main valley that hosts Pineios River runs almost parallel to the fault zone and this happens with no interruption whatsoever for the last 100 ka (Raphael, 1973). However, the downstream bend in the river toward the south appears to have

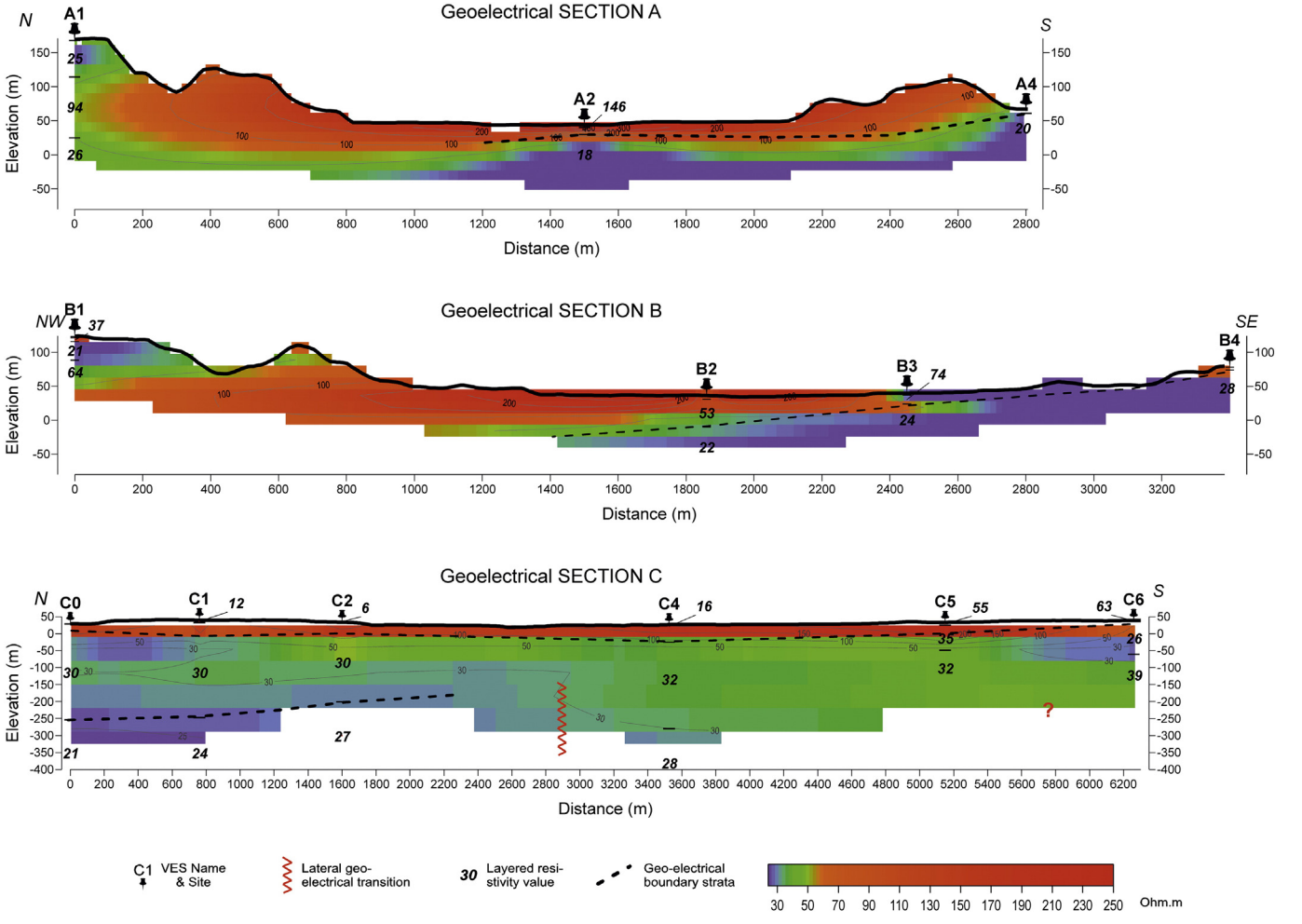

Fig. 6. Distribution of electrical resistivity along Sections A, B and C (scale 1:2).

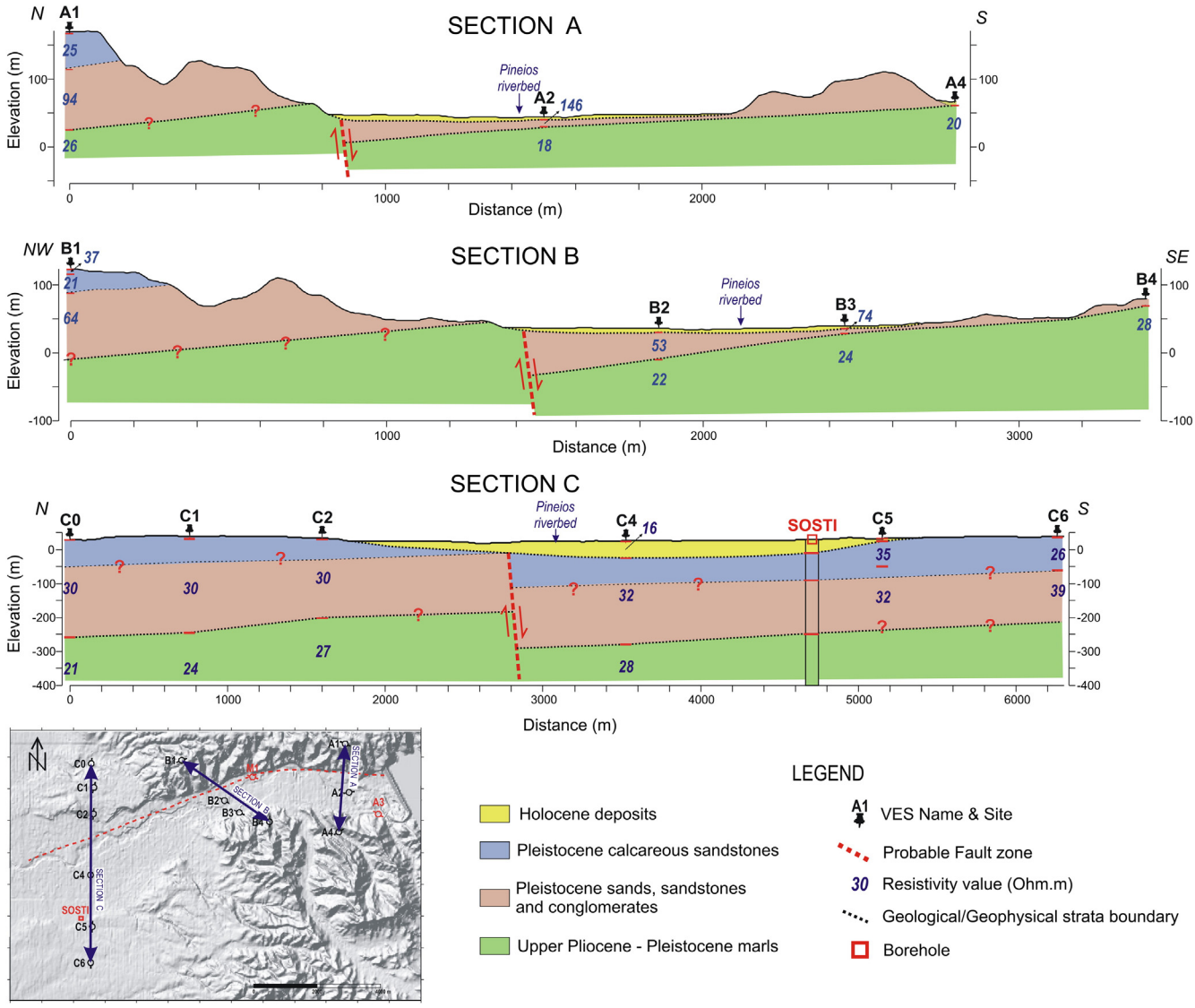

Fig. 7. Geological interpretation of the geophysical sections presented in Fig. 6 (scale 1:2). The topography is illustrated on the inset map. See Fig. 1 for site location.

changed over the last 2000 years (Kontopoulos and Koutsios, 2010). We argue that the main river valley used to accommodate flow into the sea by bending to the north somewhere between Markopoulo and Vartholomio (Fig. 1). This drastic change in flow pattern should have had a great impact on the shoreline where the river used to flow into the open sea (Kyllini Bay) and on the shoreline near its current estuary on the Ionian Sea. Sediment transport to both the deltaic areas has been altered over a very short transition period and the effects on the coastline must have been very significant given the low relief of the estuary areas. In such cases, the response of the shoreline is always a strong indicator of changes in sediment transport.

Kraft et al. (2005) describe the existence of a Roman-period shoreline that is several hundred meters offshore in Kyllini Bay, in agreement with the initial working hypothesis of this study. We argue that the northern coast is under severe erosion and has been retrograding since the southwards diversion of the Pineios River, which occurred around the 5th century (Kontopoulos and Koutsios, 2010). In contrast, on both sides of the new river mouth in the south, we expected coastal progradation because the amount of transported sediment has increased, at least before the late 1960s when the dam upstream started operation.

6.1. Data acquisition and preparation

We used several remote sensing datasets and topographic maps to determine whether progradation or retrogradation has occurred in the regions of the current and former deltas of the Pineios River in recent years. We traced the shorelines at several different times over a 40-year-period from the early 1970s to 2011 using (a) photogrammetrically constructed topographic maps at 1:5000 scale (1972), (b) two datasets of aerial photos (1987, 1996), and (c) a Landsat-ETM+ satellite image (1999). The older coastlines were compared to the present shoreline (2011), which was delineated with the use of high accuracy Real-Time Kinematics differential GPS (RTK-GPS).

Initially we collected the available data and created a satisfactory time series of images along the modern coastline. The oldest data available were several sheets of topographic maps acquired from HMGS whose construction was also based on photogrammetric techniques applied to aerial photographs. We used 42 overlapping air photographs, which were acquired during 1987 and generated an ortho-photo mosaic for that year. During this photogrammetric procedure a high resolution (2-meters) Digital Elevation Model was also produced and used afterwards for the ortho-rectification of a 15-meter resolution

Please cite this article as: Fountoulis, I., et al., Synergy of tectonic geomorphology, applied geophysics and remote sensing techniques reveals new data for active extensional tecton..., Geomorphology (2014), http://dx.doi.org/10.1016/j.geomorph.2014.11.016

Landsat-7 ETM+, panchromatic image, which was acquired during 1999. All the data were co-registered with a 1-meter spatial resolution ortho-photo mosaic created from the photogrammetric interpretation of aerial photographs acquired during 1996 (Fig. 8).

The image time series included mainly panchromatic data and the digital products were 8-bit gray-scale images covering most of the study area. By using digital image interpretation techniques we reconstructed the coastline for each time period. The greater challenge was to identify the exact points of contact between the seawater body and the onshore landscape and thus increase the accuracy of the measurements. This was accomplished by equalizing the image histogram and in some cases applying a threshold value, which was different for every air-photograph, depending on the orientation of the sunlight. The use of the visible portion of the electromagnetic spectrum for all the remote sensing data provided for homogeneity and objectivity.

Data acquisition was completed with a topographic survey using the technology of RTK-GPS point collection, which was done after establishing four GPS bases along the shore (Fig. 1). The first three were established along the northern coast, covering most of the coastal region where the Pineios River used to flow into the sea. The fourth station was established at the modern mouth of the Pineios River along the southern coast. The rover antenna was set up for acquiring easting and northing coordinates in the Hellenic Geodetic Reference System of 1987 (Greek Grid) projection system every 50 cm along the shoreline. The accuracy of the present coastline trace was very high because the specifications for the equipment used (TOPCON HiperPro) quote a precision better than 10 mm. The rover antenna was carried either by a person walking or, when possible, attached to vehicles driven along the shoreline. In each case the height of the antenna was measured and imported into the solution software (TOPCON Tools v.7).

6.2. Digital shoreline analysis results

The data collected were converted into polylines and projected in a Geographic Information System platform along with the digitized paleoshorelines. The best-case scenario would have been to have five different shorelines in each place but there were small and large gaps in each dataset due to lack of information or difficulties in discriminating the land from the water during image interpretation. The combination of all of the reconstructed coastlines from the remote sensing data with the RTK-GPS recorded coastline has shown that the former and the current delta fronts of the Pineios River are divided into various subareas characterized by different types, phases and rates of shoreline displacement.

We used the Digital Shoreline Analysis System (DSAS), version 4.2, which is a software extension to ESRI ArcGIS v.9.3.x published by the USGS (Thieler et al., 2009). This extension allows the user to create transects perpendicular to a baseline that parallels the modern shoreline at a given distance and to measure the relative position of any digitized portions of coastline. These measurements can be used for

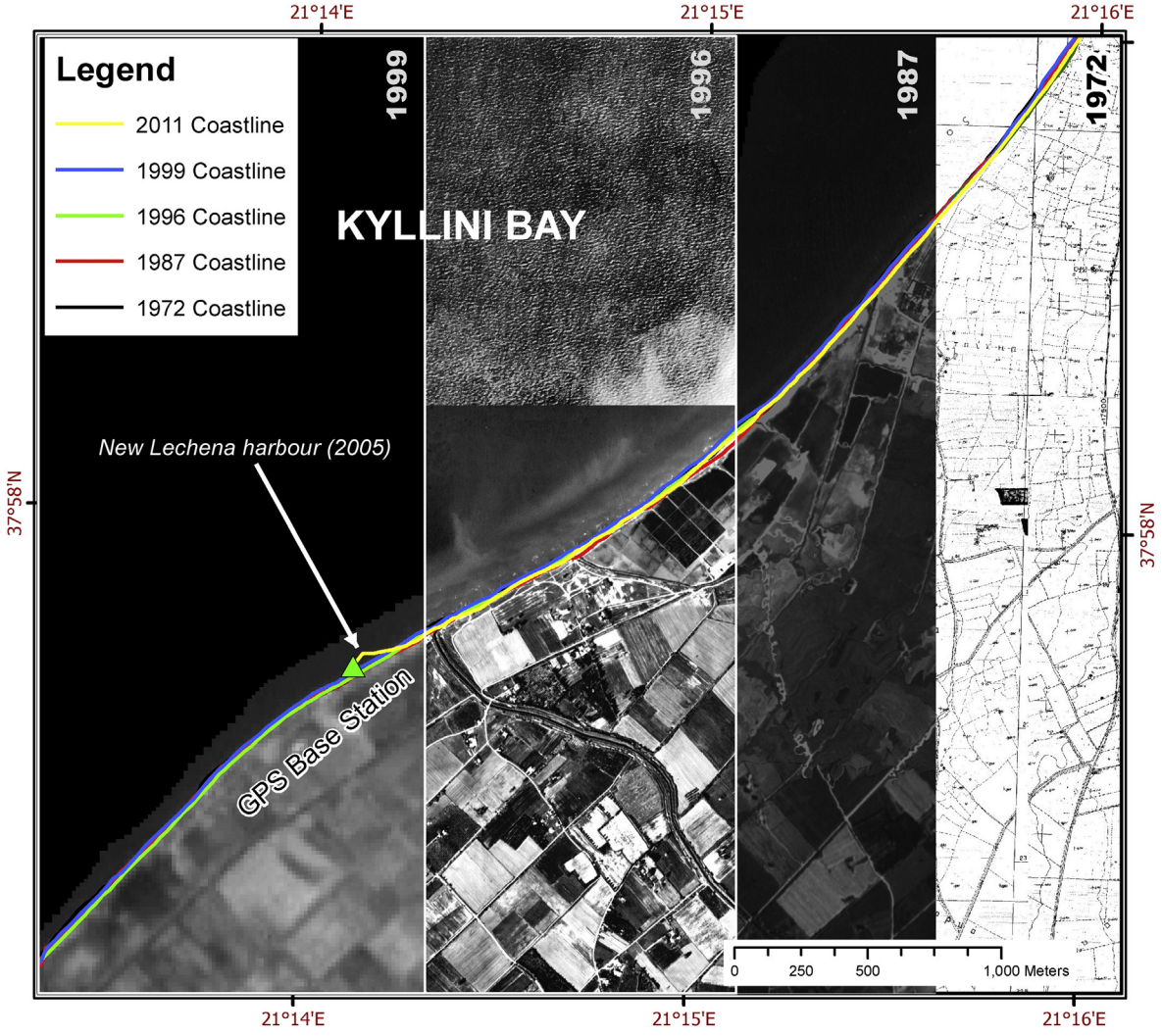

Fig. 8. Compilation of four different types of data used to trace the historical shorelines. Accuracy varies from 2 to 15 m depending on the spatial resolution of the data.

Please cite this article as: Fountoulis, I., et al., Synergy of tectonic geomorphology, applied geophysics and remote sensing techniques reveals new data for active extensional tecton..., Geomorphology (2014), http://dx.doi.org/10.1016/j.geomorph.2014.11.016

extracting the rate of change of shoreline position and other useful statistics. We defined the transect distance every 100 m along the north and south coasts with a transect length of 300 m. A point is automatically created on each transect where that transect intersects the digitized shorelines and its distance along the given baseline is measured. Using this procedure, a table of statistics containing all measured distances is generated. We used the statistics focusing along the coastal segments wherever we had more than four measurements on each transect.

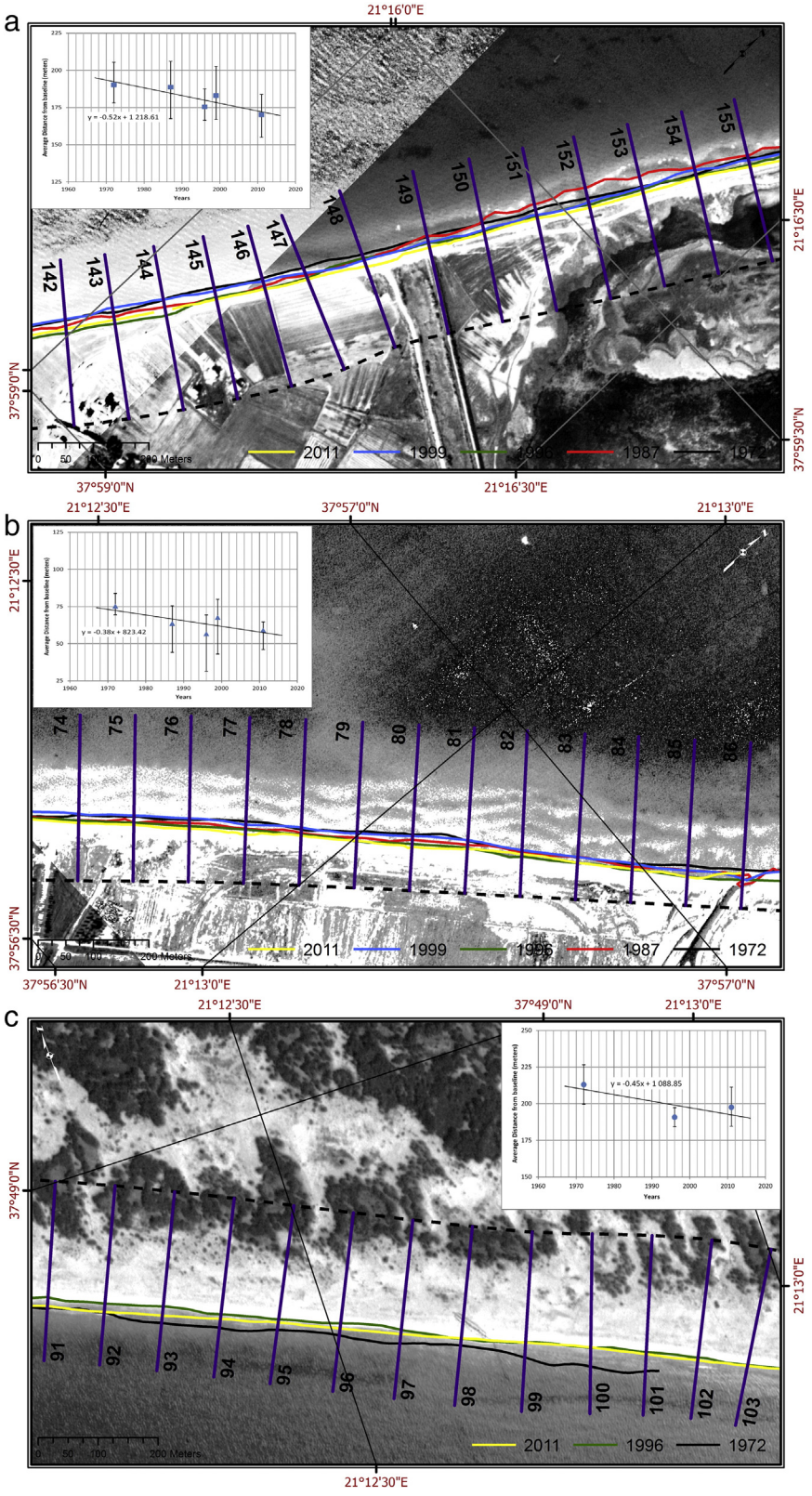

Fig. 9. Three of the most representative segments of the northern (a, b) and southern (c) coastlines. Transects located every 100 m were used to determine the rates of coastal change. Insets show the rates of coastline retrogression determined from the change in the horizontal distance of the coastline from a fixed baseline.

Please cite this article as: Fountoulis, I., et al., Synergy of tectonic geomorphology, applied geophysics and remote sensing techniques reveals new data for active extensional tecton..., Geomorphology (2014), http://dx.doi.org/10.1016/j.geomorph.2014.11.016

Throughout the total 30 km length of the northern shoreline we used a 13 km segment, which is quite representative for the northern coast. Our results define three individual areas along the northern coast. The central area shows a pattern of coastal change that is strongly affected by a small but significant port (Lechena) that was constructed a few years (harbor works completed during 2005) before the last RTK-GPS measurement (2011). The other two areas appear to display similar behavior, and to be retrograding with similar rates. The retreat rate for the northeast part of the Kyllini Bay coast is calculated to be 0.52 m/yr (Fig. 9a) while that for the southwest part is calculated to be 0.38 m/yr (Fig. 9b), which are rather similar rates. Both rates are consistent with published studies (Raphael, 1973; Kraft et al., 2005) that define the historic shoreline during the late Roman period (~1550 years BP) to be several hundreds of meters offshore from the contemporary coastline and to be somewhere between the late Roman period and modern coastlines during the Ottoman period (~400 years BP). Extrapolation of our data would predict the submerged Roman shoreline to be located 700 ± 250 m to northwest and the Ottoman shoreline to be located 190 ± 20 m to the northwest, both more or less paralleling the modern coastline.

Along the southern coastal area there appears to have been no significant human impact for the last century. Therefore the 6.5 km of RTK-GPS measurements are satisfactory although, due to lack of remote sensing data, we were able to correlate only three shorelines (1972, 1996, and 2011) and this only over a distance of 1 km, which is decent considering the homogeneous geo-environment. Although the latter calculation is not definitive because the area over which it was determined was not large, it adds to this study as a supporting piece of evidence. The average coastal retrogradation rate of the southern coastline is computed to be 0.45 m/yr after interpreting the DSAS statistic results (Fig. 9c) even if it was expected to be prograding due to the increase of sediment transportation since the estuary of Pineios River was relocated there. This value is similar to the one computed for the northern coastline. A possible explanation is that the volume of expected sediment did not reach the river's modern mouth, particularly after the dam construction upstream. This dam has been in full operation since 1968 and prevents large volumes of eroded material from reaching the modern delta. Because the oldest shoreline used in our study was made from 1972 topographic maps, it is quite possible that the presence of the dam has been responsible for the lack of progradation measured in our study.

Note that the processes that contribute to long-term shoreline change, such as the effect of sea-level rise, may have not have influenced the recent short-term shoreline changes in the same way — for example sea-level was assumed to have remained more or less constant over the last 40 years.

7. Conclusions

We combined several methodologies and several different types of data to document the presence of an unmapped active normal fault zone that strikes east–west and cuts across the area occupied by the artificial lake formed by the Pineios dam.

A geophysical survey that measured electrical resistivity along three sections perpendicular to this south-dipping normal fault zone clearly identifies this tectonic discontinuity at depth where it disrupts post-alpine strata. Interpretation of the survey results indicates that the fault throw is significantly greater in the westernmost segment of the fault zone, reaching approximately 110 m. This is in good agreement with the fault-slip rate of 0.48 mm/yr that was calculated by the differential uplift rates for blocks on either side of the fault over the past 209 ka.

The continuous activity of Pineios normal fault zone for more than 200 ka has caused relative uplift of the northern block and relative subsidence of the southern block, along with block tilting toward north. This faulting pattern has had a major impact on the river course and appears to have caused relocation of the river estuary, away from the northern uplifting fault block to the southern subsiding fault block. This has produced obvious effects on the shorelines, especially along Kyllini Bay (in the north) where submerged ancient coastlines are known. The rate of retrogradation of this shoreline, which is located on the uplifted fault block, is ~0.52 m/yr, due to Pineios River estuary migration since a major source of sediment material transportation, which would have contributed to avoid coastal erosion, has been suspended.

Acknowledgments

The author Professor Ioannis Fountoulis passed away (16/2/2013) before the publication of this article. He was a great teacher and a dear friend who left us too soon. He will always be an inspiration to us and immeasurably missed. The authors would like to express their appreciation to Prof. Leigh Royden, Dr. V. Mouslopoulou and the two anonymous reviewers whose suggestions and constructive comments highly improved the structure and the maturity of the manuscript. The geophysical survey was funded by the Special Account for Research Grants of the UoA (contract nos. 70/4/7620 & 70/4/11078).

Appendix A. Supplementary data

Supplementary data associated with this article can be found in the online version, at http://dx.doi.org/10.1016/j.geomorph.2014.11.016. These data include Google maps of the most important areas described in this article.

References

Alexopoulos, J.D., Dilalos, S., 2010. Geophysical research for geological structure determination in the region of South Mesogheia (Attica). Bull. Geol. Soc. Greece 34, 1898–1906.
Alexopoulos, J.D., Fountoulis, I., Kampouris, P., Mariolakos, I., Papadopoulos, T., 2001. Geoelectrical survey for Tatoi (Athens, Greece) blind fault. Bull. Geol. Soc. Greece 34, 121–127 (in Greek, with English Abstr.).
Asfahani, J., Radwan, Y., 2007. Tectonic evolution and hydrogeological characteristics of the Khanaser Valley, Northern Syria, derived from the interpretation of vertical electrical soundings. Pure Appl. Geophys. 164, 2291–2311.
Asfahani, J., Radwan, Y., Layyous, I., 2010. Integrated geophysical and morphotectonic survey of the impact of Ghab extensional tectonics on the Qastoon Dam, Northwestern Syria. Pure Appl. Geophys. 167, 323–338.
Athanassas, C., Fountoulis, I., 2013. Quaternary neotectonic configuration of the southwestern Peloponnese, Greece, based on luminescence ages of marine terraces. J. Earth Sci. 24, 410–427.
Athanassiou, A., 2000. Presence of fossil elephants in the area of Peniós valley (NW Peloponnesus, Greece). Ann. Géol. Pays Hellén. 38 (C), 63–76.
Brice, J.C., 1964. Channel Patterns and Terraces of the Loup Rivers in Nebraska, U.S. Geological Survey Professional Paper, 422-D, Washington (41 pp.).
Bridge, J.S., 2003. Rivers and Floodplains: Form, Process, and Sedimentary Record. Blackwell Science, Oxford (491 pp.).
Bull, W.B., 1978. Geomorphic Tectonic Activity Classes of the South Front of the San Gabriel Mountains, California. U.S. Geological Survey Contract Report 14-08-001-G-394, p. 59.
Bull, W.B., McFadden, L.D., 1977. Tectonic geomorphology north and south of the Garlock Fault, California. Geomorphology in arid regions. Proc. 8th Binghamton Symposium in, Geomorphology, pp. 115–138.
Caputo, R., 2007. Sea-level curves: perplexities of an end-user in morphotectonic applications. Glob. Planet. Chang. 57, 417–423.
Cotton, C.A., 1950. Tectonic scarps and fault valleys. Geol. Soc. Am. Bull. 61, 717–758.
Cox, R.T., 1994. Analysis of drainage basin symmetry as a rapid technique to identify areas of possible Quaternary tilt-block tectonics: an example from the Mississippi Embayment. Geol. Soc. Am. Bull. 106, 571–581.
DePolo, C.M., Anderson, J.G., 2000. Estimating the slip rates of normal faults in the Great Basin, USA. Basin Res. 12, 227–240.
Feng, L., Newman, A.V., Farmer, G.T., Psimoulis, P., Stiros, S.C., 2010. Energetic rupture, coseismic and post-seismic response of the 2008 MW 6.4 Achaia–Elia Earthquake in northwestern Peloponnese, Greece: an indicator of an immature transform fault zone. Geophys. J. Int. 183, 103–110.
Fountoulis, I., Mavroulis, S., Theocharis, D., 2007. Morphotectonic Analysis and Morphometric Indices Application in the Lefkochori–Ochthia Area (Central-Western Peloponnese, Greece), 8th Panhellenic Congress of the Geographical Society of Greece, Athens, Greece. pp. 204–214 (in Greek, with English Abstr.).
Fountoulis, I., Vassilakis, E., Mavroulis, S., Alexopoulos, J., Erkeki, A., 2011. Quantification of river valley major diversion impact at Kyllini coastal area (W. Peloponnesus, Greece) with remote sensing techniques. In: Grützner, C., Fernández Steeger, T.,

Papanikolaou, I., Reicherter, K., Silva, P.G., Pérez-López, R., Vött, A. (Eds.), 2nd INQUA-IGCP-567 International Workshop on Active Tectonics. Earthquake Geology, Archaeology and Engineering, Corinth, pp. 46–49.
Fountoulis, I., Mavroulis, S., Vassilakis, E., Papadopoulou-Vrynioti, K., 2013. Shoreline displacement and Pineios River diversions in NW Peloponnese (Greece) as result of the geology, active tectonics and human activity during the last 100 ky. Z. Geomorphol. Suppl. Issues 57, 97–123.
Garrote, J., Cox, R.T., Swann, C., Ellis, M., 2006. Tectonic geomorphology of the southeastern Mississippi Embayment in northern Mississippi, USA. Geol. Soc. Am. Bull. 118, 1160–1170.
Guidoboni, E., Comastri, A., Traina, G., 1994. Catalogue of Ancient Earthquakes in the Mediterranean Area up to the 10th Century. Instituto Nazionale di Geofisica, Roma.
Hatzfeld, D., Pedotti, G., Hatzidimitriou, P., Makropoulos, K., 1990. The strain pattern in the western Hellenic arc deduced from a microearthquake survey. Geophys. J. Int. 101, 181–202.
Holbrook, J.M., Schumm, S.A., 1999. Geomorphic and sedimentary response of rivers to tectonic deformation: a brief review and critique of a tool for recognizing subtle epeirogenic deformation in modern and ancient settings. Tectonophysics 305, 287–306.
Hollenstein, C., Geiger, A., Kahle, H.G., Veis, G., 2006. CGPS time-series and trajectories of crustal motion along the West Hellenic Arc. Geophys. J. Int. 164, 182–191.
Imbrie, J., Hays, J.D., Martinson, D.G., A, M., Mix, A.C., Morley, J.J., Pisias, N.G., Prell, W.L., Shackleton, N.J., 1984. The orbital theory of Pleistocene climate: support from a revised chronology of the marine δ18 O record. In: Berger, A., Imbrie, J., Hays, J., Kukla, G., Saltzman, B. (Eds.), Milankovitch and Climate. Reidel, Dordrecht, pp. 269–305.
Kamberis, E., 1987. Geology and Petroleum Geology Study of NW Peloponnese, Greece. (PhD Thesis), National Technical University of Athens, Greece (143 pp., in Greek).
Kamberis, E., Alexiades, X., Philipe, G., Tsaila-Monopoli, S., Ioakim, X., Tsapralis, B., 1993. Geological map of Greece, scale 1:50,000, Sheet Amalias, IGME, Athens.
Keller, E.A., Pinter, N., 1996. Active Tectonics — Earthquakes, Uplift and Landscape. Prentice Hall, New Jersey (334 pp.).
Konstantinou, K.I., Melis, N.S., Lee, S.-J., Evangelidis, C.P., Boukouras, K., 2009. Rupture process and aftershocks relocation of the 8 June 2008 Mw 6.4 earthquake in Northwest Peloponnese, Western Greece. Bull. Seismol. Soc. Am. 99, 3374–3389.
Kontopoulos, N., Koutsios, A., 2010. A late Holocene record of environmental changes from Kotihi lagoon, Elis, Northwest Peloponnesus, Greece. Quat. Int. 225, 191–198.
Koukouvelas, I.K., Kokkalas, S., Xypolias, P., 2010. Surface deformation during the Mw 6.4 (8 June 2008) Movri Mountain earthquake in the Peloponnese, and its implications for the seismotectonics of western Greece. Int. Geol. Rev. 52, 249–268.
Kraft, J.C., Rapp, G., Gifford, J.A., Aschenbrenner, S.E., 2005. Coastal Change and Archaeological Settings in Elis. Hesperia 74. American School of Classical Studies at Athens, Princeton (39 pp.).
Lekkas, E., Papanikolaou, D., Fountoulis, I., 1992. Neotectonic map of Greece, scale 1: 100,000, sheet Pyrgos–Tropaia, EPPO, Athens.
Lekkas, E., Fountoulis, I., Papanikolaou, D., 2000. Intensity distribution and neotectonic macrostructure Pyrgos Earthquake Data (26 March 1993, Greece). Nat. Hazards 21, 19–33.
Lekkas, E., Fountoulis, I., Danamos, G., Skourtsos, E., Gouliotis, L., Mavroulis, S., Kostaki, I., 2008. Seismic Fractures Related to the NW Peloponnesus (SW Greece) Earthquake (ML = 6,5R 8-6-2008), EERI, Preliminary Scientific Report (8 pp.).
Leopold, L.B., Wolman, M.G., 1957. River channel patterns: braided, meandering and straight. U.S. Geological Survey Professional Paper 282-B, Washington (85 pp.).
Margaris, B., Athanasopoulos, G.A., Mylonakis, G., Papaioannou, C., Klimis, N., Theodulidis, N., Savvaidis, A., Efthymiadou, V., Stewart, J.P., 2010. The 8 June 2008 Mw 6.5 Achaia–Elia, Greece earthquake: source characteristics, ground motions, and ground failure. Earthquake Spectra 26, 399–424.
Mariolakos, I., Papanikolaou, D., Lagios, E., 1985. A neotectonic geodynamic model of Peloponnesus based on morphotectonics, repeated gravity measurements and seismicity. Geol. Jahrb. B50, 3–17.
Mariolakos, I., Lekkas, E., Danamos, G., Logos, E., Fountoulis, I., Adamopoulou, E., 1991. Neotectonic evolution of the Kyllini Peninsula (NW Peloponnese, Greece). Bull. Geol. Soc. Greece 25, 163–176 (in Greek, with English Abstr.).
Mavroulis, S., 2009. Fault Activity Assessment in NW Peloponnesus — The Andravida Earthquake (08/06/2008). (MSc Thesis), National and Kapodistrian University of Athens, Greece (622 pp., in Greek).
Mavroulis, S., Fountoulis, I., Lekkas, E., 2010. Environmental effects caused by the Andravida (08-06-2008, ML = 6.5, NW Peloponnese, Greece) earthquake. In: Williams, A., Pinches, G., Chin, C., McMorran, T., Massey, C. (Eds.), Geologically Active: 11th IAEG Congress. Taylor & Francis Group, Auckland, New Zealand, pp. 451–459.
Mavroulis, S.D., Fountoulis, I.G., Skourtsos, E.N., Lekkas, E.L., Papanikolaou, I.D., 2013. Seismic intensity assignments for the 2008 Andravida (NW Peloponnese, Greece) strike-slip event (June 8, Mw = 6.4) based on the application of the Environmental Seismic Intensity scale (ESI 2007) and the European Macroseismic scale (EMS-98). Geological structure, active tectonics, earthquake environmental effects and damage pattern. Ann. Geophys. 56. http://dx.doi.org/10.4401/ag-6239.
Menges, C.M., 1990. Late Quaternary fault scarps, mountain-front landforms, and Pliocene–Quaternary segmentation on the range-bounding fault zone, Sangre de Cristo Mountains, New Mexico. In: Krinitzsky, E., Slemmons, D. (Eds.), Neotectonics in Earthquake Evaluation. Geological Society of America Reviews in Engineering Geology, Boulder, Colorado, pp. 131–156.
Ouchi, S., 1985. Response of alluvial rivers to slow active tectonic movement. Geol. Soc. Am. Bull. 96, 504–515.
Papadopoulos, T., Goulty, N., Voulgaris, N.S., Alexopoulos, J.D., Fountoulis, I., Kambouris, P.J., Karastathis, V., Peirce, C., Chailas, S., Kassaras, J., Pirli, M., Goumas, G., Lagios, E., 2007. Tectonic structure of Central-Western Attica (Greece) based on geophysical investigations—preliminary results. Bull. Geol. Soc. Greece 40, 1207–1218.
Papadopoulos, G.A., Karastathis, V., Kontoes, C., Charalampakis, M., Fokaefs, A., Papoutsis, I., 2010. Crustal deformation associated with east Mediterranean strike-slip earthquakes: the 8 June 2008 Movri (NW Peloponnese), Greece, earthquake (Mw6.4). Tectonophysics 492, 201–212.
Papanikolaou, D., 1984. The three metamorphic belts of the Hellenides; a review and a kinematic interpretation. In: Dixon, J.E., Robertson, A.H.F. (Eds.), The geological evolution of the eastern Mediterranean. Geological Society of London Spec. Publ 17, pp. 551–561.
Papanikolaou, D., 1997. The tectonostratigraphic terranes of the Hellenides. Ann. Géol. Pays Hellén. 37, 495–514.
Papanikolaou, D., Fountoulis, I., Metaxas, C., 2007. Active faults, deformation rates and Quaternary paleogeography at Kyparissiakos Gulf (SW Greece) deduced from onshore and offshore data. Quat. Int. 171–172, 14–30.
Papazachos, B.C., Papazachou, C.B., 1997. The Earthquakes of Greece. Ziti Publications, Thessaloniki (304 pp.).
Paraskevaidis, I., Symeonidis, N., 1965. Beitrag zur Kenntnis der Stratigraphie des Neogen von West Peloponnes. Ann. Géol. Pays Hellén. 16, 528–544.
Ramírez-Herrera, M.T., 1998. Geomorphic assessment of active tectonics in the Acambay graben, Mexican Volcanic Belt. Earth Surf. Process. Landf. 23, 317–332.
Raphael, C.N., 1973. Late Quaternary changes in Coastal Elis, Greece. Geogr. Rev. 63, 73–89.
Rockwell, T.K., Keller, E.A., Johnson, D.L., 1984. Tectonic geomorphology of alluvial fans and mountain fronts near Ventura, California. In: Morisawa, M., Hack, T.J. (Eds.), Tectonic Geomorphology. State University of New York, Binghamton, pp. 183–207.
Rust, B.R., 1978. A classification of alluvial channel systems. In: Miall, A.D. (Ed.), Fluvial Sedimentology, Canadian Society of Petroleum Geologists, Memoir 5, pp. 187–198.
Schumm, S.A., 1963. Sinuosity of alluvial rivers on the Great Plains. Geol. Soc. Am. Bull. 74, 1089–1100.
Shackleton, J.C., Andel, T.H.v, Runnels, C.N., 1984. Coastal paleogeography of the Central and Western Mediterranean during the last 125,000 years and its archaeological implications. J. Field Archaeol. 11, 307–314.
Silva, P.G., Goy, J.L., Zazo, C., Bardají, T., 2003. Fault-generated mountain fronts in southeast Spain: geomorphologic assessment of tectonic and seismic activity. Geomorphology 50, 203–225.
Stamatopulos, L., Voltaggio, M., Kontopulos, N., Cinque, A., La Rocca, S., 1988. $^{230}Th/^{238}U$ dating of corals from Tyrrhenian marine deposits of Varda area (North-western Peloponnesus), Greece. Geogr. Fis. Dinam. Quat. 11, 99–103.
Symeonidis, N., Therodorou, G., 1986. New locations of fossil Hippopotamus in northwest Peloponnese. Ann. Géol. Pays Hellén. 33, 51–67.
Thenius, E., 1955. Hippopotamus aus dem Astien von Elis (Peloponnes). Ann. Géol. Pays Hellén. 6, 206–212.
Theocharis, D., Fountoulis, I., 2002. Morphometric Indices and Tectonically Active Structures: The Case of Salamis Island, 6th Panhellenic Geographical Congress, Geographic Society of Greece. pp. 97–106 (in Greek, with English Abstr.).
Thieler, E., Himmelstoss, E., Zichichi, J., Ergul, A., 2009. Digital Shoreline Analysis System (DSAS) version 4.0—an ArcGIS extension for calculating shoreline change. U.S. Geological Survey Open-file Report 2008-1278.
Underhill, J.R., 1988. Triassic evaporites and Plio-Quaternary diapirism in western Greece. J. Geol. Soc. 145, 269–282.
Vassilakis, E., Royden, L., Papanikolaou, D., 2011. Kinematic links between subduction along the Hellenic trench and extension in the Gulf of Corinth, Greece: a multidisciplinary analysis. Earth Planet. Sci. Lett. 303, 108–120.
Waelbroeck, C., Labeyrie, L., Michel, E., Duplessy, J.C., McManus, J.F., Lambeck, K., Balbon, E., Labracherie, M., 2002. Sea-level and deep water temperature changes derived from benthic foraminifera isotopic records. Quat. Sci. Rev. 21, 295–305.
Wallace, R., 1977. Profiles and ages of young fault scarps, north-central Nevada. Geol. Soc. Am. Bull. 88, 1267–1281.
Wells, S.G., Bullard, T.F., Menges, C.M., Drake, P.G., Karas, P.A., Kelson, K.I., Ritter, J.B., Wesling, J.R., 1988. Regional variations in tectonic geomorphology along a segmented convergent plate boundary pacific coast of Costa Rica. Geomorphology 1, 239–265.
Zámolyi, A., Székely, B., Draganits, E., Timár, G., 2010. Neotectonic control on river sinuosity at the western margin of the Little Hungarian Plain. Geomorphology 122, 231–243.
Zohdy, A.A.R., 1989. A new method for the automatic interpretation of Schlumberger and Wenner sounding curves. Geophysics 54, 245–253.

Please cite this article as: Fountoulis, I., et al., Synergy of tectonic geomorphology, applied geophysics and remote sensing techniques reveals new data for active extensional tecton..., Geomorphology (2014), http://dx.doi.org/10.1016/j.geomorph.2014.11.016